CHINESE OPTICS LETTERS

Vol. 20, No. 2 | February 2022

High performance optical sensor based on double compound symmetric gratings

Chaoying Shi (史超颖)[1], Xiuhong Liu (刘秀红)[1*], Jinhua Hu (胡劲华)[2], Haiyan Han (韩海燕)[1], and Jijun Zhao (赵继军)[2]

[1] School of Mathematics & Physics, Hebei University of Engineering, Handan 056038, China

[2] School of Information & Electrical Engineering, Hebei University of Engineering, Handan 056038, China

*Corresponding author: liuxiuhong@hebeu.edu.cn

Received July 8, 2021 | Accepted August 17, 2021 | Posted Online October 8, 2021

A high performance optical sensor based on a double compound symmetric gratings (DCSGs) structure is designed. The reflection spectrum of the DCSG is investigated by utilizing a method that combines a theoretical model with the eigenmode information of the grating structure. The theoretical results, which are observed to agree well with those acquired by rigorous coupled-wave analysis, show that the linewidth of the reflection spectrum decreases upon the increasing distance between the grating strips. This research work will lay a foundation for studying high performance integrated optical sensors in miniature nanostructures.

Keywords: compound gratings; sensitivity; sensor; figure of merit.

DOI: 10.3788/COL202220.021201

1. Introduction

Optical biosensors are needed in many fields, such as biomolecular testing[1,2], chemical analyses[3], and environmental monitoring[4]. Many kinds of optical technologies have been proposed to achieve high performance optical biosensors in recent years, including surface plasmon resonance (SPR)[5] and guided-mode resonance (GMR) biosensors, typically. In 1993, Wang and Magnusson discovered the GMR effect of periodic waveguide gratings[6]. This effect means that when the phase of the incident light wave matches the guiding mode of the grating, a sharp resonant peak will appear in the output spectrum due to the modulation of the grating structure. In 2000, a new type of GMR device integrating a waveguide grating with a subwavelength period on the endface of an optical fiber was proposed by Wawro *et al.*[7]. In addition, the advantages of no fluorescent labeling, easy integration, and real-time detection have made GMR-based grating sensors widely used in biomedical sensing[8,9]. In 2005, Magnusson *et al.* described the characteristics of GMR and demonstrated their utility in biosensors[10]. However, for now, GMR-based grating sensors still have some shortcomings. Some cannot be adapted to high sensitivity detection environments because of low sensitivity[11,12]; some have difficulty achieving high performance optical sensing owing to low figure of merit (FOM)[13,14]. On the other hand, the complex structure and demanding fabrication process make it difficult to achieve mass production of these devices. In order to solve these problems, we have designed an optical sensor based on a double compound symmetric gratings (DCSGs) structure, which simply means that a compound waveguide grating (CWG) structure is added to a dual-grating (DG) structure[15].

CWG structures are often designed to reduce the bandwidth of the resonant peaks for devices[16]. Nevertheless, unlike the previous CWGs that used a single-layer compound structure[17,18], the performance of the sensor has been further improved thanks to our use of a double-layer compound structure. More differently, we use the identical optical material so that the grating has the same refractive index. But the waveguide layer of conventional gratings is basically made of optical materials with a high refractive index[19], which, to a certain extent, increases the complexity of the manufacturing. There are many methods to fabricate GMR devices, such as electron beam lithography, laser interference lithography, and nanoimprint lithography[20]. Patterns on a given stamp can be transferred to resist or other imprint materials by nanoimprint lithography, and then heat or UV light can accomplish the curing process[21]. Nanoimprint lithography offers cost-effective parallel nanofabrication that is fast, simple, reproducible, and qualified for mass production. The optical adhesive Norland Optical Adhesive 73 (NOA73) with a refractive index of 1.56 is chosen as the material for our grating structure. NOA73 is a flexible material that exhibits low shrinkage and cures to a solid under UV light[22], so the fabrication process is not only simplified by nanoimprint lithography, but also mass production is possible. A device with a DC structure was fabricated in this way by Hemmati *et al.* in 2019[21].

In this Letter, a DCSG-based structure is proposed in order to better improve the performance of the sensor. Then, the device structure is designed by the rigorous coupled-wave algorithm (RCWA)[23,24], and the effect of the grating spacing variation on the sensor performance is mainly analyzed. On this basis, eigenmode information of the grating structure is determined through the finite element method (FEM), and then the reflection spectrum is calculated by combining the theoretical model in Ref. [25], the results of which are able to match well with the RCWA results. Therefore, we can explain the variation of the resonant peaks in terms of the eigenmode, since the spectral shape of the resonance is directly determined by the eigenvalue of the mode.

2. Structure and Theory

Figure 1 shows a schematic diagram of the proposed DCSG-based optical sensor structure, which contains four separate and identical grating strips (two at the top and two at the bottom) in each period. Additionally, the structure is completely symmetrical and entirely covered by a liquid with a refractive index of n_c. The material used throughout the grating is NOA73 with a refractive index of 1.56. The DCSG is considered to be infinite in the y-direction and periodic in the x-direction. The parameters of the proposed sensor are as follows: the period of the compound gratings is Λ, the grating filling factor is f, the width and height of the four identical grating strips in each period are w and L, respectively, the interspacing between the two grating strips in each period is d, and the homogeneous film thickness is h. In our proposed model, the DCSG is viewed as a single-mode resonator. The eigenmode of the grating structure is determined by FEM simulation, and the reflection spectrum is then calculated using the theoretical model.

In this method, a single period of the DCSG structure is defined as a unit cell, and NOA73 can be considered lossless. First, we use the FEM to calculate the eigenmode information of the resonant grating structure. During the simulation, we choose Floquet periodic boundary conditions as the lateral boundary conditions, while the upper and lower boundaries use scattering boundary conditions[26]. Then, the eigenmode of the resonant grating structure can be obtained having the form $N = N_{\mathrm{real}} - iN_{\mathrm{imag}}$, where N_{real} and N_{imag} are the real and imaginary parts of N, respectively, and the central resonance frequency ω_0 and the quality factor q_0 of GMR can be obtained using[27]

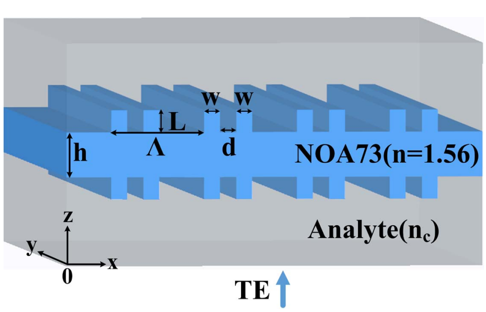

Fig. 1. Schematic of the sensor based on the DCSG structure.

$$\begin{cases} \omega_0 = N_{\mathrm{real}} \\ q_0 = N_{\mathrm{real}}/2\,N_{\mathrm{imag}} \end{cases}. \tag{1}$$

According to the effective medium theory, the effective refractive index N_{eff} can be defined as[28]

$$N_{\mathrm{eff}} = \sqrt{n_c^2(1-f)^2 + n^2 f}, \tag{2}$$

where n_c is the refractive index of the analyte, n is 1.56, and f is the grating filling factor. So the reflection spectrum of the resonator can be obtained based on the relation[25]

$$R = 1 - \left| t - \frac{(t+r)N_{\mathrm{imag}}}{i(\omega - N_{\mathrm{real}}) + N_{\mathrm{imag}}} \right|^2, \tag{3}$$

where N_{real} and N_{imag} are the real and imaginary parts of N, respectively, and ω is the resonance frequency. The DCSG structure is considered to be a uniform slab waveguide with the same thickness and effective refractive index, so its amplitude reflection coefficient r and transmission coefficient t can be calculated[29].

The sensitivity (S) and FOM are usually utilized to evaluate the performance of the sensor and can be expressed as[30]

$$S = \frac{\Delta\lambda_{\mathrm{res}}}{\Delta n_c}, \tag{4}$$

$$\mathrm{FOM} = \frac{S}{\Delta\lambda}, \tag{5}$$

where $\Delta\lambda_{\mathrm{res}}$ is the resonance wavelength shift, Δn_c is the change in n_c, and $\Delta\lambda$ is the full width at half-maximum (FWHM).

3. Results and Discussion

First, we compared the spectral response of the DG and DCSG using the RCWA, as shown in Fig. 2. We assumed the following structural parameters for the DCSG: $\Lambda = 980$ nm, $L = 250$ nm, $h = 1000$ nm, $f = 0.45$, $d = 260$ nm, and $w = 220.5$ nm ($w = f \times \Lambda/2$). $d = 0$ for the DG structure. TE polarized light was used

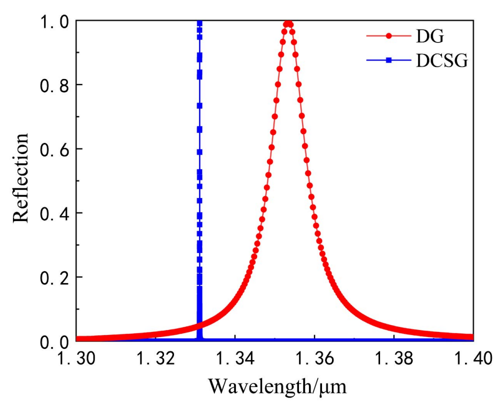

Fig. 2. Reflection spectra of DG and DCSG at normal incidence of TE waves.

Table 1. Eigenvalues of the TE Eigenmode with Different d.

d (nm)	Eigenvalue N
200	$1.4136 \times 10^{15} - 4.41132 \times 10^{11} i$
220	$1.4144 \times 10^{15} - 2.30627 \times 10^{11} i$
240	$1.4151 \times 10^{15} - 8.93895 \times 10^{10} i$
260	$1.4154 \times 10^{15} - 1.92105 \times 10^{10} i$

as the incident light source and was incident normally. Figure 2 shows a sharp narrowing of the FWHM and a blue shift of the resonance peak when the compound structure is introduced. To illustrate the effect of the parameter d on the performance of the sensor, we performed a detailed analysis when $d = 200, 220, 240$, and 260 nm. The FEM was used to calculate the eigenvalues for different d, which are listed in Table 1.

According to Eq. (1) and Table 1, the central resonant frequencies and quality factors of the DCSG structure can be obtained. It can be seen that the real part of the eigenvalues exhibits a small variation with increasing d, while the imaginary part decreases sharply. This indicates a very significant improvement in the quality factor of the DCSG structure as d increases. The physical meaning of the quality factor in a resonator is expressed as the ratio of stored energy to the consumed energy. As the spacing between the two grating strips increases, the amount of energy stored within the optical resonator is increasing. This further illustrates the increasing confinement capability of the grating structure for incident light waves.

To further understand the physical properties of this eigenmode, we simulated the electric field intensity distributions for different d in each cell of the DCSG structure by using the FEM, the results of which are shown in Fig. 3. It can be seen that as d increases, more of the electric field is confined between the two grating strips.

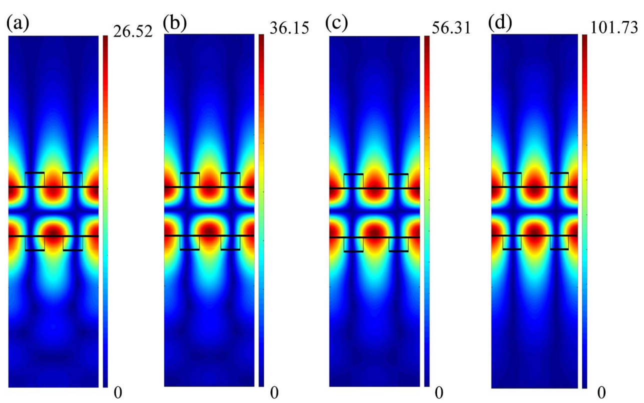

Fig. 3. Electric field intensity distributions of the eigenmode in different DCSGs with various spacings: (a) d = 200 nm, (b) d = 220 nm, (c) d = 240 nm, (d) d = 260 nm.

Next, the reflectance spectrum of different d at TE polarization is calculated by using Eq. (3), as shown in Fig. 4. In Fig. 4, we compared the calculated reflection spectrum with the simulated results of RCWA, showing that the calculated spectrum is in good agreement with the simulated results. Our calculations show that it is feasible to analyze and predict spectral line shape variations with the help of eigenmodes.

Finally, the performance indicators of the designed DCSG structure sensor were analyzed. Its sensitivity and FOM are calculated by Eqs. (4) and (5), respectively. The sensing performance parameters of the DCSG structure with different d are calculated in Table 2. It can be seen that the FWHM decreases by a factor of approximately 54 as d changes from 200 nm to 260 nm. However, the increase in sensitivity is not significant. This is explained by the fact that there is a trade-off between sensitivity and FOM in the GMR-based sensors[31,32]. It can be seen from Fig. 3 that the electric field energy increases from 26.52 to 101.73 as the d increases, and most of the light is confined inside the grating region. For the proposed structure, the FOM is improved without sacrificing its sensitivity. Physically, a high FOM is obtained when the resonant FWHM is reduced, which can increase the spectral discrimination of the biosensor. For the proposed DCSG structure in Fig. 1, the coupling between the

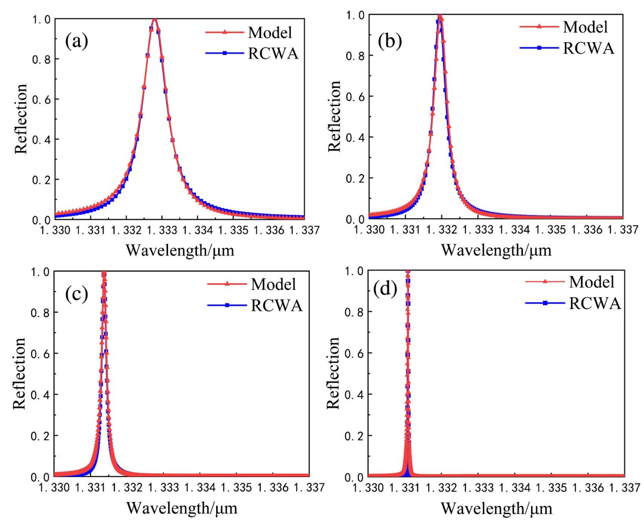

Fig. 4. Reflection responses of the DCSG for the TE polarization with different d: (a) d = 200 nm, (b) d = 220 nm, (c) d = 240 nm, (d) d = 260 nm.

Table 2. FWHM, S, and FOM of Structures for Different d in TE Mode.

d (nm)	FWHM (nm)	S (nm/RIU)	FOM
200	0.811	461	568
220	0.414	469	1133
240	0.146	471	3226
260	0.015	472	31,467

Table 3. Eigenvalues of TE Eigenmodes Corresponding to Different Refractive Indices.

Refractive Index n_c	Eigenvalue N
1.331	$1.4154 \times 10^{15} - 1.92115 \times 10^{10} i$
1.333	$1.4136 \times 10^{15} - 2.0212 \times 10^{10} i$
1.335	$1.4126 \times 10^{15} - 2.1336 \times 10^{10} i$
1.337	$1.4115 \times 10^{15} - 2.2593 \times 10^{10} i$
1.339	$1.4105 \times 10^{15} - 2.2399 \times 10^{10} i$

compound gratings can be controlled by adjusting the spacing between the two grating strips, where a larger distance implies a weaker coupling, which leads to a reduction in the spectral width. Therefore, an optical sensor with a high FOM value can be obtained by controlling the spacing between the compound gratings.

By the analysis in Table 2, the other structural parameters of the grating remain unchanged, with $d = 260$ nm chosen. As the refractive index of the analyte is changed from 1.331 to 1.339, its eigenvalue is calculated by FEM, as listed in Table 3.

It can be noticed that when d changes from 1.331 to 1.339, a red shift of the resonance peak can be seen according to Eq. (1). To further verify the results of the eigenvalue analysis, the reflectance spectrum was calculated using RCWA as n_c increased from 1.331 to 1.339, and the results are shown in Fig. 5. It shows that the resonance peak has red shift with increasing analyte refractive index, and the FWHM remains almost unchanged. The central wavelength of the GMR grating structure is related to the resonant condition. A change in the refractive index of the analyte will change the conditions under which the GMR is generated[33,34]. As a result, the position of the resonant reflection peak will be shifted with the varied refractive indices of the analyte.

Further analysis of the fitted curve as the position of the resonance peak varies with analyte refractive index shows a linear relationship between the resonance wavelength and the

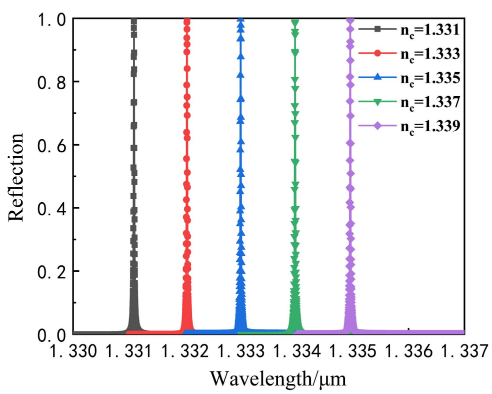

Fig. 5. DCSG reflection spectra for TE polarization with different n_c.

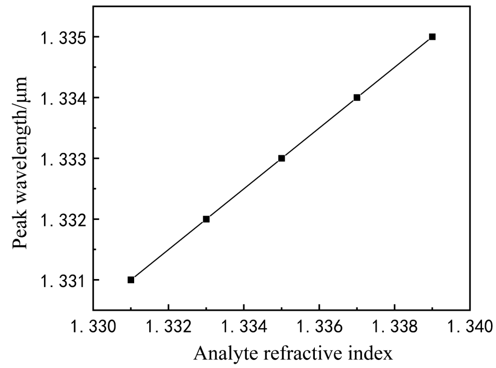

Fig. 6. DCSG resonance peak wavelength versus n_c.

refractive index, which can be seen in Fig. 6. Based on the above results, we can obtain a high performance optical sensor with a sensitivity of 472 nm/RIU and an FOM of 31,476.

4. Conclusion

In conclusion, a DCSG-based optical sensor is proposed, concentrating on the performance of the device at different compound spacings. By changing the spacing between the compound gratings, the eigenmode of the grating can be regulated, changing the magnitude of the eigenvalue to achieve the purpose of regulating the reflectance spectral linewidth and optimizing the performance of the sensor. The theoretical simulation results show that the sensitivity of the sensor is 472 nm/RIU, the FWHM is only 0.015 nm, and the FOM value is 31,467. The research work in this Letter provides a reference for the design of new grating sensors.

Acknowledgement

This work was supported in part by the National Natural Science Foundation of China (Nos. 61905060 and 21976049), Natural Science Foundation of Hebei Province (Nos. F2019402063 and F2019402240), and Scientific Research Project of the Department of Education of Hebei Province (No. ZD2021019).

References

1. S. Kumar and R. Singh, "Recent optical sensing technologies for the detection of various biomolecules: review," Opt. Las. Tech. **134**, 106620 (2021).
2. Y. Moreno, Q. G. Song, Z. K. Xing, Y. Z. Sun, and Z. J. Yan, "Hybrid tilted fiber gratings-based surface plasmon resonance sensor and its application for hemoglobin detection," Chin. Opt. Lett. **18**, 100601 (2020).
3. S. Sen and K. Ahmed, "Design of terahertz spectroscopy based optical sensor for chemical detection," SN Appl. Sci. **1**, 1215 (2019).
4. B. Chocarro-Ruiz, A. Fernandez-Gavela, S. Herranz, and L. M. Lechuga, "Nanophotonic label-free biosensors for environmental monitoring," Curr. Opin. Biotech. **45**, 175 (2017).
5. X. B. Wang, H. C. Deng, and L. B. Yuan, "High sensitivity cascaded helical-core fiber SPR sensors," Chin. Opt. Lett. **19**, 091201 (2021).
6. S. S. Wang and R. Magnusson, "Theory and applications of guided-mode resonance filters," Appl. Opt. **32**, 14 (1993).

7. D. Wawro, S. Tibuleac, R. Magnusson, and H. Liu, "Optical fiber endface biosensor based on resonances in dielectric waveguide gratings," Proc. SPIE **3911**, 86 (2000).
8. R. Magnusson, K. J. Lee, H. Hemmati, Y. H. Ko, B. R. Wenner, J. W. Allen, M. S. Allen, S. Gimlin, and D. W. Weidanz, "The guided-mode resonance biosensor: principles, technology, and implementation," Proc. SPIE **10510**, 105100G (2018).
9. A. Kenaan, K. Z. Li, I. Barth, S. Johnson, J. Song, and T. F. Krauss, "Guided mode resonance sensor for the parallel detection of multiple protein biomarkers in human urine with high sensitivity," Biosen. Bioelec. **153**, 112047 (2020).
10. R. Magnusson, Y. Ding, K. J. Lee, P. S. Priambodo, and D. Wawro, "Characteristics of resonant leaky mode biosensors," Proc. SPIE **6008**, 60080U (2005).
11. Y. F. Ku, H. Y. Li, W. H. Hsieh, L. K. Chau, and G. E. Chang, "Enhanced sensitivity in injection-molded guided-mode-resonance sensors via low-index cavity layers," Opt. Express **23**, 14850 (2015).
12. S. Boonruang and W. S. Mohammed, "Multiwavelength guided mode resonance sensor array," Appl. Phys. Express **8**, 092004 (2015).
13. L. Wang, T. Sang, J. L. Li, J. Y. Zhou, B. X. Wang, and Y. K. Wang, "High-sensitive transmission type of gas sensor based on guided-mode resonance in coupled gratings," J. Mod. Opt. **65**, 1601 (2018).
14. Y. Zhou, X. S. Li, S. A. Li, Z. Guo, P. Zeng, J. B. He, D. C. Wang, R. J. Zhang, M. Lu, S. Y. Zhang, and X. Wu, "Symmetric guided-mode resonance sensors in aqueous media with ultrahigh figure of merit," Opt. Express **27**, 34788 (2019).
15. D. A. Bykov, E. A. Bezus, and L. L. Doskolovich, "Coupled-wave formalism for bound states in the continuum in guided-mode resonant gratings," Phys. Rev. A **99**, 063805 (2019).
16. J. H. Hu, Y. Q. Huang, X. M. Ren, X. F. Duan, Y. H. Li, Q. Wang, X. Zhang, and J. Wang, "Modeling of Fano resonance in high-contrast resonant grating structures," Chin. Phys. Lett. **31**, 064205 (2014).
17. H. Lu, M. Huang, X. B. Kang, W. X. Liu, C. Dong, J. Zhang, S. Q. Xia, and X. Z. Zhang, "Improving the sensitivity of compound waveguide grating biosensor via modulated wavevector," Appl. Phys. Express **11**, 082202 (2018).
18. W. X. Liu, Y. H. Li, H. T. Jiang, Z. Q. Lai, and H. Chen, "Controlling the spectral width in compound waveguide grating structures," Opt. Lett. **38**, 163 (2013).
19. I. D. Block, N. Ganesh, M. Lu, and B. T. Cunningham, "A sensitivity model for predicting photonic crystal biosensor performance," IEEE. Sens. J. **8**, 3 (2008).
20. G. Quaranta, G. Basset, O. J. F. Martin, and B. Gallinet, "Recent advances in resonant waveguide gratings," Las. Photon. Rev. **12**, 1800017 (2018).
21. H. Hemmati and R. Magnusson, "Resonant dual-grating metamembranes supporting spectrally narrow bound states in the continuum," Adv. Opt. Mater. **7**, 1900754 (2019).
22. H. Hemmati and R. Magnusson, "Development of tuned refractive-index nanocomposites to fabricate nanoimprinted optical devices," Opt. Mater. Express **8**, 175 (2018).
23. M. G. Moharam, E. B. Grann, and D. A. Pommet, "Formulation for stable and efficient implementation of the rigorous coupled-wave analysis of binary gratings," J. Opt. Soc. Am. A **12**, 1068 (1995).
24. M. G. Moharam, D. A. Pommet, and E. B. Grann, "Stable implementation of the rigorous coupled-wave analysis for surface-relief gratings: enhanced transmittance matrix approach," J. Opt. Soc. Am. A **12**, 1077 (1995).
25. S. H. Fan, W. Suh, and J. D. Joannopoulos, "Temporal coupled-mode theory for the Fano resonance in optical resonators," J. Opt. Soc. Am. A **20**, 569 (2003).
26. N. Komarevskiy, V. Shklover, L. Braginsky, and C. Hafner, "Ultrasensitive switching between resonant reflection and absorption in periodic gratings," Prog. Electrom. Res. **139**, 799 (2013).
27. Y. L. Yu and L. Y. Cao, "Coupled leaky mode theory for light absorption in 2D, 1D, and 0D semiconductor nanostructures," Opt. Express. **20**, A13 (2012).
28. S. M. Rytov, "Electromagnetic properties of a finely stratified medium," Sov. Phys. JETP **2**, 466 (1956).
29. S. H. Fan and J. D. Joannopoulos, "Analysis of guided resonances in photonic crystal slabs," Phys. Rev. B **65**, 235112 (2002).
30. J. H. Hu, X. H. Liu, J. J. Zhao, and J. Zou, "Investigation of Fano resonance in compound resonant waveguide gratings for optical sensing," Chin. Opt. Lett. **15**, 030502 (2017).
31. A. Szeghalmi, E. B. Kley, and M. Knez, "Theoretical and experimental analysis of the sensitivity of guided mode resonance sensors," J. Phys. Chem. C **114**, 21150 (2010).
32. L. Wang, T. Sang, J. Gao, X. Yin, and H. L. Qi, "High-performance sensor achieved by hybrid guide-mode resonance/surface plasmon resonance platform," Appl. Opt. **57**, 7338 (2018).
33. Y. N. Bao, H. X. Liu, J. H. Hu, H. Y. Han, Q. F. Zhu, S. X. Xi, and J. Z. Yu, "High performance optical refractive index sensor based on concave resonant grating," Chin. J. Laser. **48**, 0913001 (2021).
34. G. L. Lan, S. Zhang, H. Zhang, Y. H. Zhu, L. Y. Qing, D. M. Li, J. P. Nong, W. Wang, L. Chen, and W. Wei, "High-performance refractive index sensor based on guided-mode resonance in all-dielectric nano-silt array," Phy. Lett. A **383**, 1478 (2019).